# Effects of Anisotropic Turbulent Ocean on Propagation of Asymmetric Bessel-Gaussian Beam

Lin Yu, Zhecheng Zhang, Yixin Zhang, and Lifa Hu

***Abstract*—Aiming at the propagation of asymmetric vortex beam, we investigate the spreading and wander characteristics of asymmetric Bessel-Gaussian beam in oceanic turbulence. Based on the cross-spectral density and Wigner distribution function of beam field, the theoretical expressions of spreading factor and beam center displacement are established to evaluate spreading and wander. The anisotropic turbulent condition is adopted to analyze turbulence impacts with more generality. The turbulence dominated by salinity fluctuation with lower anisotropy, larger temperature dissipation and smaller kinetic energy dissipation induces more beam spreading and wander. As for asymmetric Bessel-Gaussian beam, the increment of asymmetry can improve beam directionality. Besides, smaller beam scale but larger Gaussian waist radius, vortex order and beam wavelength also mitigate spreading and wander. The investigations are instructive for the underwater applications of asymmetric vortex beams.**

***Index Terms*—Asymmetric Bessel-Gaussian beam, beam propagation, oceanic turbulence, optical vortex.**

## I. Introduction

THE propagation properties of various beams in turbulent media have been researched widely in recent years for applications of free space optical communication and optical imaging [1]. The random fluctuations of refractive index of turbulent media cause laser wavefront distortion and degrade beam propagation quality [2]. Among different negative effects induced by turbulent media, beam spreading and wander affect beam size and center position at the receiver [3], [4]. The spreading of beam spot and the displacement of beam center increase difficulties to beam receiving within a specific aperture and beam focusing in detection using fiber coupling. Investigations on the characteristics of beam spreading and wander in turbulent media are helpful to the optimal design of optical systems.

In previous reports, Cui et al. analyzed the spreading and wander of Gaussian wave in atmospheric turbulence, and discussed the effects of turbulence scale and spectral power law value [5]. Taking laser array into consideration, Zhang et al. investigated the propagation factor and wander of electromagnetic Gaussian Schell-model array beams in turbulent atmosphere. The polarization and coherence of beams were considered [6]. Aiming at the partially coherent Airy beam, Jin et al. investigated the relative beam wander to beam width in isotropic oceanic turbulence [7]. Ata et al. analyzed the effects of the average temperature and average salinity concentration on the spreading and wander of Gaussian beam based on a new oceanic turbulence optical power spectrum [8].

Later, with the development of multiplexing technology based on optical orbital angular momentum, vortex beams became a research focus [9]. Zhu et al. derived the theoretical expression of long-term beam width for Bessel-Gaussian beam in turbulent atmosphere, and simulated the evolution of propagation factor [10]. Luo et al. investigated the single collimated vortex beam and radial vortex beam array. The key factors affecting intensity distribution and beam spreading were discussed [11]. Singh et al. analyzed the wander of ring Pearcey vortex beam in turbulent atmosphere and found that it had smaller wander than ring Airy vortex beam [12]. Falits et al. investigated the wander of optical vortex through artificial convective turbulence experimentally and analyzed the effect of topological charge [13]. Yang et al. extended the research from traditional Laguerre-Gaussian beam to perfect Laguerre-Gaussian beam, and analyzed beam spreading and wander in isotropic turbulent absorbent seawater [14].

Based on the explorations on conventional circular symmetric vortex beams, asymmetric vortex beams were generated gradually [15], [16]. Asymmetric Bessel-Gaussian beam is one typical asymmetric vortex beam, which is constructed by introducing an asymmetric factor into the linear superposition of Bessel-Gaussian beams [15]. The transverse field distribution and orbital angular momentum carried by asymmetric Bessel-Gaussian beam can be adjusted by the asymmetric factor, which gives more flexibility for beam optimization in different applications. In terms of asymmetric Bessel-Gaussian beam, Dai et al. reported its experimental generation using second harmonic conversion and obtained orbital angular momentum of both integer and fractional orders [17]. Wu et al. derived the analytical expression of optical field amplitude in nonparaxial case and simulated the variation of axial intensity with propagation distance [18]. Yu et al. analyzed vortex modal crosstalk and calculated signal detection probability and channel capacity [19]. However, as important factors affecting propagation quality, the spreading and wander of asymmetric Bessel vortex in turbulence haven't been reported yet. Different from the previous researches on symmetric vortex beams, the spreading and wander in condition of asymmetric vortex field are worthy to be investigated.

Manuscript received 26 October 2023; revised 12 December 2023; accepted 31 December 2023. Date of publication 4 January 2024; date of current version 16 January 2024. This work was supported by the National Natural Science Foundation of China under Grants 11904136, 11847109, and 61871202. *(Corresponding author: Lin Yu.)*

The authors are with the School of Science, Jiangnan University, Wuxi 214122, China, and also with the Jiangsu Provincial Research Center of Light Industrial Optoelectronic Engineering and Technology, Wuxi 214122, China (e-mail: yulin@jiangnan.edu.cn; 6221206038@stu.jiangnan.edu.cn; zyx@jiangnan.edu.cn; hulifa@jiangnan.edu.cn).

Digital Object Identifier 10.1109/JPHOT.2024.3349706

Considering the more generalized oceanic turbulent condition with anisotropy is also useful for the development of beam propagation underwater.

In this paper, we focus on the spreading and wander of asymmetric Bessel-Gaussian beam in the propagation medium of anisotropic turbulent ocean. The cross-spectral density perturbed by oceanic turbulence is derived to obtain the Wigner distribution function of beam field. Based on the moments of Wigner distribution function in spatial domain, the theoretical expressions of beam width and center displacement are established to evaluate beam spreading and wander. Lastly, numerical simulations are conducted to analyze the turbulence effects. The way for beam parameter optimization is also discussed to improve propagation performance.

## II. Cross-Spectral Density of Asymmetric Bessel-Gaussian Beam

As the solution of Helmholtz equation in free space, asymmetric Bessel-Gaussian beam is essentially the linear superposition of conventional Bessel-Gaussian beams. The complex amplitude of asymmetric Bessel-Gaussian beam at the source plane is described as [15]

$$E(\boldsymbol{r_0},0)=\sum_{p=0}^{\infty}\frac{c^p}{p!}J_{m+p}(\alpha k\, r_0)\exp\left(-\frac{r_0^2}{w_0^2}\right)\times\exp\left[i\,(m+p)\,\varphi_0\right], \tag{1}$$

where $\boldsymbol{r_0}=(r_0\cos\varphi_0, r_0\sin\varphi_0)$ is the position vector determined by radius $r_0$ and angle $\varphi_0$, $k=2\pi\, n_{oc}/\lambda$ is beam wavenumber in ocean, $n_{oc}$ and $\lambda$ correspond to the oceanic refractive index and beam wavelength in vacuum respectively, $\alpha$ is beam scale factor given by the sine of Bessel cone angle, $m$ is beam order, $c$ is the asymmetry factor, $w_0$ is the waist radius of Gaussian envelope, $J_{m+p}(\cdot)$ is the $(m+p)$th order Bessel function of the first kind and $p$ is an integral.

Fig. 1 shows the transverse field distribution of asymmetric Bessel-Gaussian beam at the source plane under different beam parameters. When the modulus of complex number $c$ increases, the transverse beam field deviates from circular symmetry gradually and asymmetry enhances. The argument of $c$ determines the orientation of peak amplitude by giving the rotation angle of peak position relative to $x$ axis in clockwise direction. For the special case of $c=0$, the asymmetry field degenerates into the conventional Bessel-Gaussian form. Besides of $c$, $m$ and $\alpha$ are also important factors affecting beam field distribution. With the increment of $m$ and decrement of $\alpha$, the central bright ring spreads. As a result, the initial beam width at the source plane becomes larger although $w_0$ keeps invariant.

To obtain the cross-spectral density of asymmetric Bessel-Gaussian beam, we rewrite the term of Bessel function in (1) for the convenience of subsequent derivations. By use of the following integral formula related to Bessel function [20]:

$$\int_0^{2\pi}\exp\left[in\theta+i\tau\cos(\theta-\varphi)\right]d\theta=2\pi\, i^n\, J_n(\tau)\exp(in\varphi)[n\in N], \tag{2}$$

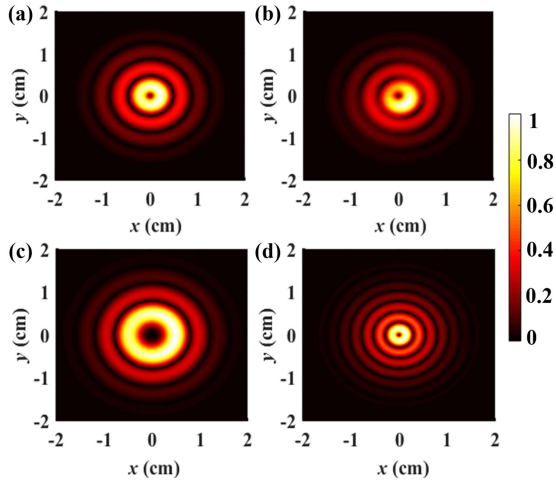


Fig. 1. Transverse field of asymmetric Bessel-Gaussian beam. Compared with the beam parameters $c=0.1$, $m=1$, $\alpha=0.00005$, $n_{oc}=1.33$, $\lambda=520$ nm and $w_0=0.01$m in (a), the different beam parameters in (b), (c) and (d) are respectively $c=0.5\exp(i\pi/4)$, $m=3$ and $\alpha=0.00008$.

the cross-spectral density at the source place is expressed as

$$W(\boldsymbol{r_{01}},\boldsymbol{r_{02}},0)=E(\boldsymbol{r_{01}},0)\,E^*(\boldsymbol{r_{02}},0)$$
$$=\frac{1}{4\pi^2}\sum_{p=0}^{\infty}\sum_{p'=0}^{\infty}\frac{c^p\,(c^*)^{p'}}{p!p'!}\exp\left[-\frac{r_{01}^2+r_{02}^2}{w_0^2}\right]$$
$$\times\int_0^{2\pi}\int_0^{2\pi}\exp\left[i\,(m+p)\,\theta-i(m+p')\theta'\right]$$
$$\times\exp\left\{i\alpha k\left[r_{01}\cos(\theta-\varphi_{01})-r_{02}\cos(\theta'-\varphi_{02})\right]\right\}d\theta d\theta'. \tag{3}$$

Referring to the usual ways of variable substitution in multiple integral, two vectors $\boldsymbol{r_{0s}}=(\boldsymbol{r_{01}}+\boldsymbol{r_{02}})/2$ and $\boldsymbol{r_{0d}}=\boldsymbol{r_{01}}-\boldsymbol{r_{02}}$ are defined to substitute $\boldsymbol{r_{01}}$ and $\boldsymbol{r_{02}}$. So (3) is rewritten as

$$W(\boldsymbol{r_{0s}},\boldsymbol{r_{0d}},0)=\frac{1}{4\pi^2}\sum_{p=0}^{\infty}\sum_{p'=0}^{\infty}\frac{c^p\,(c^*)^{p'}}{p!p'!}\int_0^{2\pi}\int_0^{2\pi}W_{\theta\theta'}(\boldsymbol{r_{0s}},\boldsymbol{r_{0d}},0)$$
$$\times\exp[i\,(m+p)\,\theta-i(m+p')\theta']d\theta d\theta', \tag{4}$$

$$W_{\theta\theta'}(\boldsymbol{r_{0s}},\boldsymbol{r_{0d}},0)=\exp\left[-2\frac{\boldsymbol{r_{0s}^2}}{w_0^2}-\frac{1}{2}\frac{\boldsymbol{r_{0d}^2}}{w_0^2}+i\left(\boldsymbol{r_{0s}}\cdot\boldsymbol{k_-}+\frac{1}{2}\,\boldsymbol{r_{0d}}\cdot\boldsymbol{k_+}\right)\right], \tag{5}$$

where the vector terms $\boldsymbol{k_+}$ and $\boldsymbol{k_-}$ have forms of $\boldsymbol{k_\pm}=\alpha k(\cos\theta\pm\cos\theta',\sin\theta\pm\sin\theta')$.

Then based on the extended Huygens-Fresnel principle, the cross-spectral density at the receiving plane is expressed as

$$W(\boldsymbol{r_s},\boldsymbol{r_d},z)=\frac{1}{4\pi^2}\sum_{p=0}^{\infty}\sum_{p'=0}^{\infty}\frac{c^p\,(c^*)^{p'}}{p!p'!}\int_0^{2\pi}\int_0^{2\pi}W_{\theta\theta'}(\boldsymbol{r_s},\boldsymbol{r_d},z)$$

$$\times \exp[i\,(m+p)\,\theta - i(m+p')\theta']d\theta d\theta', \tag{6}$$

$$W_{\theta\theta'}\left(\boldsymbol{r_s}, \boldsymbol{r_d}, z\right) = \left(\tfrac{k}{2\pi z}\right)^2 \int_{-\infty}^{\infty}\int_{-\infty}^{\infty}\int_{-\infty}^{\infty}\int_{-\infty}^{\infty} d^2\,\boldsymbol{r_{0s}}\, d^2\,\boldsymbol{r_{0d}}\, W_{\theta\theta'}\left(\boldsymbol{r_{0s}}, \boldsymbol{r_{0d}}, 0\right) \times \exp\left[\frac{ik}{z}\left(\boldsymbol{r_s}-\boldsymbol{r_{0s}}\right)\cdot\left(\boldsymbol{r_d}-\boldsymbol{r_{0d}}\right)\right]\exp\left[\psi(\boldsymbol{r_d}, \boldsymbol{r_{0d}}, z)\right], \tag{7}$$

where the variables $\boldsymbol{r_s} = (\boldsymbol{r_1}+\boldsymbol{r_2})/2$ and $\boldsymbol{r_d} = \boldsymbol{r_1}-\boldsymbol{r_2}$ have similar relationships with the position vectors $\boldsymbol{r_1}$ and $\boldsymbol{r_2}$ as those at the source plane, $z$ is the propagation distance, the exponential term $\exp[\psi(\boldsymbol{r_d}, \boldsymbol{r_{0d}}, z)]$ introduces turbulence effect into beam propagation.

By substituting (5) into (7), the further result of $W_{\theta\theta'}$ $(\boldsymbol{r_s}, \boldsymbol{r_d}, z)$ can be obtained. With the introduction of an intermediate variable $\boldsymbol{\kappa_d}$ and help of the following integral formulae [20]:

$$\delta(\boldsymbol{r'_{0s}} - \boldsymbol{r_{0s}}) = \tfrac{1}{(2\pi)^2}\int_{-\infty}^{\infty}\int_{-\infty}^{\infty}\exp\left[i\,\boldsymbol{\kappa_d}\cdot(\boldsymbol{r'_{0s}}-\boldsymbol{r_{0s}})\right]d^2\,\boldsymbol{\kappa_d}$$

$$\int_{-\infty}^{\infty}\exp\left(-a^2\,x^2+bx\right)\mathrm{d}x = \frac{\sqrt{\pi}}{a}\exp\left(\frac{b^2}{4\,a^2}\right)(a>0), \tag{8}$$

the simplified expression of $W_{\theta\theta'}(\boldsymbol{r_s}, \boldsymbol{r_d}, z)$ is derived after some integral operations similar to the derivations in [10], [21]. The result is given by

$$W_{\theta\theta'}\left(\boldsymbol{r_s}, \boldsymbol{r_d}, z\right) = \frac{w_0^2}{8\pi}\int_{-\infty}^{\infty}\int_{-\infty}^{\infty}\exp\left[-\frac{w_0^2}{8}\,\boldsymbol{k}_-^2 - \frac{1}{2}\frac{\boldsymbol{r_d^2}}{w_0^2} + \frac{i}{2}\,\boldsymbol{k}_+\cdot\boldsymbol{r_d} + \left(\frac{iz}{2k}\,\boldsymbol{k}_+ - \frac{z}{k\,w_0^2}\,\boldsymbol{r_d} - \frac{w_0^2}{4}\,\boldsymbol{k}_- - i\,\boldsymbol{r_s}\right)\cdot\boldsymbol{\kappa_d} - \left(\frac{w_0^2}{8}+\frac{z^2}{2\,k^2\,w_0^2}\right)\boldsymbol{\kappa_d^2} + \psi\left(\boldsymbol{r_d}, \boldsymbol{r_d}+\frac{z}{k}\,\boldsymbol{\kappa_d}, z\right)\right]d^2\,\boldsymbol{\kappa_d}. \tag{9}$$

According to Rytov approximation, the turbulence effect on beam field can be regarded as complex phase perturbation, which is related to turbulence features, propagation distance and beam wavenumber. The form is [2]

$$\psi\left(\boldsymbol{r_d}, \boldsymbol{r_d}+\frac{z}{k}\,\boldsymbol{\kappa_d}, z\right) = -4\,\pi^2\,k^2\,z\int_0^1 d\xi\int_0^{\infty}\Phi(\kappa)\kappa \times\left[1-J_0\left(\kappa\left|(1-\xi)\,\boldsymbol{r_d} + \xi\left(\boldsymbol{r_d}+z\,\boldsymbol{\kappa_d}/k\right)\right|\right)\right]\mathrm{d}\kappa, \tag{10}$$

where $\kappa$ is the spatial frequency, $\Phi(\kappa)$ reflects turbulence features and gives the power spectrum of refractive index fluctuations. In the paraxial case with the truncation of $J_0(x) = 1 - x^2/4$, (10) is simplified as

$$\psi\left(\boldsymbol{r_d}, \boldsymbol{r_d}+\frac{z}{k}\,\boldsymbol{\kappa_d}, z\right) = -\frac{3}{\rho_c^2}\int_0^1\left|\boldsymbol{r_d}+\frac{z}{k}\xi\,\boldsymbol{\kappa_d}\right|^2\mathrm{d}\xi, \tag{11}$$

$$\rho_c = \left[\frac{1}{3}\pi^2k^2z\int_0^{\infty}\kappa^3\Phi(\kappa)d\kappa\right]^{-1/2}, \tag{12}$$

where $\rho_c$ is the spatial coherence radius of beam in turbulent medium. As for anisotropic turbulence ocean, $\Phi(\kappa)$ can be described by Nikishov's spectrum as [22]

$$\begin{aligned}\Phi(\kappa) &= 0.388\times10^{-8}\chi_T\varepsilon^{-1/3}\zeta^2\,\kappa_\zeta^{-11/3}\\ &\quad\times\left[1+2.35(\kappa_\zeta\,\eta)^{2/3}\right]f(\kappa_\zeta)\\ f(\kappa_\zeta) &= \exp\left[-A_T\,f'(\kappa_\zeta)\right] - 2\varpi^{-1}\exp\left[-A_{TS}\,f'(\kappa_\zeta)\right]\\ &\quad+\varpi^{-2}\exp\left[-A_S\,f'(\kappa_\zeta)\right]\\ f'(\kappa_\zeta) &= 8.284(\kappa_\zeta\,\eta)^{4/3}+12.978(\kappa_\zeta\,\eta)^2,\end{aligned} \tag{13}$$

where $\chi_T$ and $\varepsilon$ are the dissipation rates of temperature and kinetic energy respectively, $\varpi$ is the temperature-salinity contribution ratio to turbulence, $\eta$ is the inner scale of turbulence eddies and $\zeta$ is the anisotropic factor. Since the axial spatial frequency $\kappa_z$ can be neglected according to the Markov approximation of random medium, the relationship between $\kappa_\zeta$ and $\kappa$ is described by $\kappa = \sqrt{\kappa_\rho^2+\kappa_z^2} \approx \kappa_\rho$ and $\kappa_\zeta = \sqrt{\zeta^2\,\kappa_\rho^2+\kappa_z^2} \approx \zeta\kappa$. $A_T$, $A_S$ and $A_{TS}$ are three constants related to temperature effect, salinity effect and temperature-salinity co-effect of turbulence respectively, whose values are $A_T = 1.863\times10^{-2}$, $A_S = 1.9\times10^{-4}$ and $A_{TS} = 9.41\times10^{-3}$.

By substituting (13) into (12) and making the integral calculation, the analytical expression of $\rho_c$ has the form of [23]

$$\rho_c = \zeta\left|\varpi\right|\left[1.802\times10^{-7}k^2z(\varepsilon\eta)^{-1/3}\chi_T \times(0.483\varpi^2-0.835\varpi+3.380)\right]^{-1/2}. \tag{14}$$

## III. Spreading and Wander of Asymmetric Bessel-Gaussian Beam

When asymmetric Bessel-Gaussian beam propagates in turbulent ocean, beam spreads due to factors of diffraction and turbulence. The beam width at the receiver can be given by the moments of Wigner distribution function. Based on the beam cross-spectral density, the expression of Wigner distribution function $h(\boldsymbol{r_s}, \boldsymbol{\vartheta}, z)$ is written as [21], [24]

$$h\left(\boldsymbol{r_s}, \boldsymbol{\vartheta}, z\right) = \tfrac{k^2}{4\,\pi^2}\int_{-\infty}^{\infty}\int_{-\infty}^{\infty}W\left(\boldsymbol{r_s}, \boldsymbol{r_d}, z\right)\exp(-ik\,\boldsymbol{r_d}\cdot\boldsymbol{\vartheta})\,d^2\,\boldsymbol{r_d}, \tag{15}$$

where the vector $\boldsymbol{\vartheta}$ denotes the direction of transverse wave vector at the receiving plane. Then the second-order moment $\langle x^2\rangle + \langle y^2\rangle$ of Wigner distribution function in spatial domain

can be further calculated as

$$\langle x^2\rangle + \langle y^2\rangle = \frac{\int_{-\infty}^{\infty}\int_{-\infty}^{\infty}\int_{-\infty}^{\infty}\int_{-\infty}^{\infty}\left(x^2+y^2\right)h(\boldsymbol{r_s},\boldsymbol{\vartheta},z)\,d^2\,\boldsymbol{r}_s\,d^2\,\boldsymbol{\vartheta}}{\int_{-\infty}^{\infty}\int_{-\infty}^{\infty}\int_{-\infty}^{\infty}\int_{-\infty}^{\infty}h(\boldsymbol{r_s},\boldsymbol{\vartheta},z)\,d^2\,\boldsymbol{r}_s\,d^2\,\boldsymbol{\vartheta}}. \tag{16}$$

During the substitution of (6) and (15) into (16), if we define two variables $H_{nn'}$ and $S_{nn'}$ as follows:

$$H_{nn'} = \frac{k^2}{4\,\pi^2}\int_{-\infty}^{\infty}\int_{-\infty}^{\infty}\int_{-\infty}^{\infty}\int_{-\infty}^{\infty}\int_{-\infty}^{\infty}\int_{-\infty}^{\infty} x^n y^{n'} \times W_{\theta\theta'}\left(\boldsymbol{r}_s,\boldsymbol{r_d},z\right)\exp(-ik\,\boldsymbol{r_d}\cdot\boldsymbol{\vartheta})\,d^2\,\boldsymbol{r_d}\,d^2\,\boldsymbol{r}_s\,d^2\,\boldsymbol{\vartheta}, \tag{17}$$

$$S_{nn'} = \frac{1}{4\,\pi^2}\sum_{p=0}^{\infty}\sum_{p'=0}^{\infty}\frac{c^p\,(c^*)^{p'}}{p!p'!}\int_0^{2\pi}\int_0^{2\pi} H_{nn'} \times \exp[i\,(m+p)\,\theta - i(m+p')\theta']d\theta d\theta', \tag{18}$$

the expression of $\langle x^2\rangle + \langle y^2\rangle$ is simplified. Then the long-term beam width $w_l$ at the receiver, which can be described as the root-mean-square of the term $\langle x^2\rangle + \langle y^2\rangle$, is written as

$$w_l(z) = \sqrt{\langle x^2\rangle + \langle y^2\rangle} = \sqrt{(S_{20}+S_{02})/S_{00}}. \tag{19}$$

After substituting (9) and (11) into (17), we conduct the integral calculations with the help of the following integral formula [20]:

$$\delta^{(n)}(x) = \frac{1}{2\pi}\int_{-\infty}^{\infty}(-it)^n\exp(-ixt)\mathrm{d}t(n=0,1,2), \tag{20}$$

where $\delta^{(n)}(x)$ is the derivative of Dirac delta function. The result is given by

$$H_{00} = \frac{1}{2}\pi\,w_0^2\exp\left(-\frac{w_0^2\,\boldsymbol{k}_-^2}{8}\right)$$

$$H_{20}+H_{02} = \left(\frac{w_0^2}{2}+\frac{2\,z^2}{k^2\,w_0^2}+\frac{4\,z^2}{k^2\,\rho_c^2}+\frac{z^2\,\boldsymbol{k}_+^2}{4k^2}-\frac{w_0^4\,\boldsymbol{k}_-^2}{16}\right) \times\frac{1}{2}\pi\,w_0^2\exp\left(-\frac{w_0^2\,\boldsymbol{k}_-^2}{8}\right). \tag{21}$$

Then substituting (18) and (21) into (19) (see Appendix), the analytical expression of long-term beam width $w_l$ is obtained as

$$w_l(z) = \left[\frac{w_0^2}{2}-\frac{w_0^4}{8}\,\alpha^2\,k^2+\left(\frac{\alpha^2}{2}+\frac{2}{k^2\,w_0^2}+\frac{4}{k^2\,\rho_c^2}\right)z^2 + \left(\frac{\alpha^2\,z^2}{4}+\frac{\alpha^2\,k^2\,w_0^4}{16}\right)\frac{F_{m+1}+F_{m-1}}{F_m}\right]^{-1/2}$$

$$F_m = \sum_{p=0}^{\infty}\frac{|c|^{2p}}{p!^2}\,I_{m+p}\left(\frac{\alpha^2\,k^2\,w_0^2}{4}\right), \tag{22}$$

where $I_{m+p}(\cdot)$ is the $(m+p)$th order modified Bessel function of the first kind.

Considering that the initial beam width at the source plane ($z=0$) is affected by beam parameters, we introduce the spreading factor defined as

$$w_r(z) = w_l(z)/w_l(0). \tag{23}$$

$w_r$ gives the relative value of beam width at the receiver and transmitter, which can be used to describe the spreading of asymmetric Bessel-Gaussian beam in turbulent ocean.

Besides of beam spreading, the instantaneous center of vortex beam experiences random displacement due to the effects of turbulence. The root-mean-square displacement $r_c$ is usually used to evaluate beam wander. Based on the theoretical expression of long-term beam width, $r_c$ can be calculated as [2]

$$r_c = \left[8\,\pi^2\,z^2\int_0^z\left(1-\frac{\sigma}{z}\right)^2 R(\sigma)\mathrm{d}\sigma\right]^{-1/2}, \tag{24}$$

$$R(\sigma) = \int_0^{\infty}\kappa^3\Phi(\kappa)\exp\left[-\kappa^2\,w_l^2(\sigma)\right]\mathrm{d}\kappa. \tag{25}$$

By substituting (13) into (25) and making the integral operation (see Appendix), the analytical expression of $R(\sigma)$ is written as

$$\mathrm{R}(\sigma) = 10^{-8}\chi_T\varepsilon^{-1/3}\zeta^{-2}(A_1 - 2A_2\varpi^{-1}+A_3\varpi^{-2}), \tag{26}$$

$$A_i = \eta^{2/3}(0.808\,V_i^{-1/2} - 0.423\,U_i\,V_i^{-7/6} + 0.2144\,U_i^2\,V_i^{-11/6}) + 1.08\,V_i^{-1/6} - 0.219\,U_i\,V_i^{-5/6} + 0.086\,U_i^2\,V_i^{-3/2}(i=1,2,3), \tag{27}$$

$$U_1 = 0.1543\eta^{4/3}, U_2 = 0.078\eta^{4/3},$$
$$U_3 = 0.00157\eta^{4/3}, V_1 = 0.242\eta^2+\zeta^{-2}\,w_l^2(\sigma),$$
$$V_2 = 0.122\eta^2+\zeta^{-2}\,w_l^2(\sigma), V_3 = 0.00247\eta^2+\zeta^{-2}\,w_l^2(\sigma). \tag{28}$$

Then substituting (26)–(28) and (22) into (24), $r_c$ can be calculated numerically to investigate the wander of asymmetric Bessel-Gaussian beam.

## IV. Results and Discussions

In this section, the oceanic turbulence effects on the spreading and wander of asymmetric Bessel-Gaussian beam are analyzed first. Then aiming at the beam itself, the variations of spreading factor and center displacement with different beam parameters are researched, based on which the ways to mitigate beam spreading and wander in turbulent ocean are discussed. In the following numerical simulations, some typical values of beam and turbulence parameters are adopted [15], [25], [26]. They are $\chi_T = 10^{-8}\,\mathrm{K}^2/\mathrm{s}$, $\varepsilon = 10^{-6}\,\mathrm{m}^2/\mathrm{s}^3$, $\eta = 1$ mm, $\varpi = -2$, $\zeta = 2$, $n_{oc} = 1.33$, $z = 100$ m, $\alpha = 0.00005$, $m = 1$, $c = 0.5$, $w_0 = 0.01$ m and $\lambda = 520$ nm if not specified.

Fig. 2 shows the spreading factor $w_r$ and center displacement $r_c$ of asymmetric Bessel-Gaussian beam under different temperature dissipation rates $\chi_T$ and kinetic energy dissipation rates $\varepsilon$ of oceanic turbulence. The ranges of $\chi_T$ and $\varepsilon$ are selected to make the turbulence conditions cover from weak turbulence to strong turbulence by use of Rytov variance to distinguish

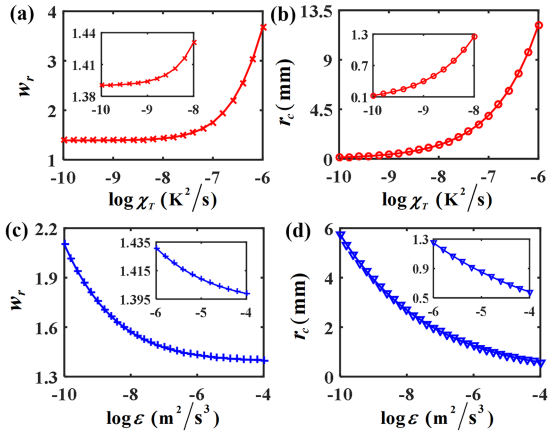


Fig. 2. Influences of temperature dissipation rate $\chi_T$ and kinetic energy dissipation rate $\varepsilon$ on the (a), (c) spreading and (b), (d) wander of asymmetric Bessel-Gaussian beam.

turbulence strength [27]. The results reveal that $w_r$ and $r_c$ become larger when $\chi_T$ increases or $\varepsilon$ decreases. The influences of $\chi_T$ on beam spreading and wander are more significant than those of $\varepsilon$. Similar to the concept of structure constant in atmospheric turbulence, the term $C_n^2 = 10^{-8}\chi_T\varepsilon^{-1/3}$ in the power spectrum of oceanic turbulence can be regarded as the equivalent [4]. Since $C_n^2$ reflects the temperature induced refractive index fluctuations, the increment of $\chi_T$ or decrement of $\varepsilon$ in fact causes the enhancement of turbulence. As a result, the asymmetric Bessel-Gaussian beam suffers more perturbations during propagation and has larger spreading and wander. Moreover, $\chi_T$ and $\varepsilon$ vary with the depth of ocean, whose values at deeper location are usually smaller than those at shallower location [28]. From the view of mitigating beam spreading and wander, constructing the beam transmitting and receiving link in deeper water is preferable.

To consider the effects of temperature and kinetic energy dissipation rates simultaneously, Fig. 3 investigates the spreading factor $w_r$ and center displacement $r_c$ under different structure constants $C_n^2$ of oceanic turbulence. With the increment of $C_n^2$, both $w_r$ and $r_c$ increase because turbulence enhances. If two turbulent conditions have different $\chi_T$ and $\varepsilon$ but the same $C_n^2$, the spreading and wander of asymmetric Bessel-Gaussian beam propagating in them are at the same level. Apart from temperature fluctuation, oceanic turbulence also contains salinity fluctuation. The temperature-salinity contribution ratio $\varpi$ makes influences on $w_r$ and $r_c$. When $\varpi$ varies towards its lower limit of $-5$, the temperature fluctuation contributes more to oceanic turbulence [22]. On the contrary, the salinity fluctuation contributes more when $\varpi$ varies towards its upper limit of 0. Although $w_r$ and $r_c$ increase with $\varpi$ monotonously, their increments are much faster in turbulence region where salinity fluctuation is dominant distinctly. This is because the further increment of $\varpi$ larger than $-1$ causes rapid enhancement of turbulence strength due to large Rytov variance [27]. As a result, the oceanic turbulence dominated by salinity fluctuation brings more perturbations on asymmetric Bessel-Gaussian beam and induces larger spreading and wander.

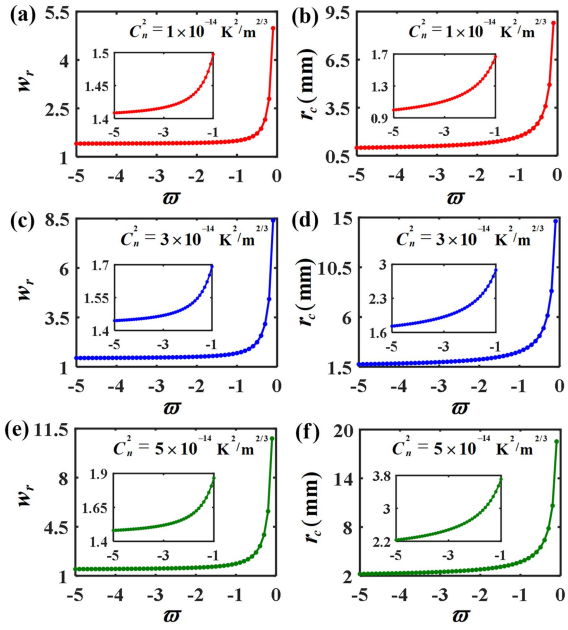


Fig. 3. Influences of structure constant $C_n^2$ and temperature-salinity contribution ratio $\varpi$ on the (a), (c), (e) spreading and (b), (d), (f) wander of asymmetric Bessel-Gaussian beam.

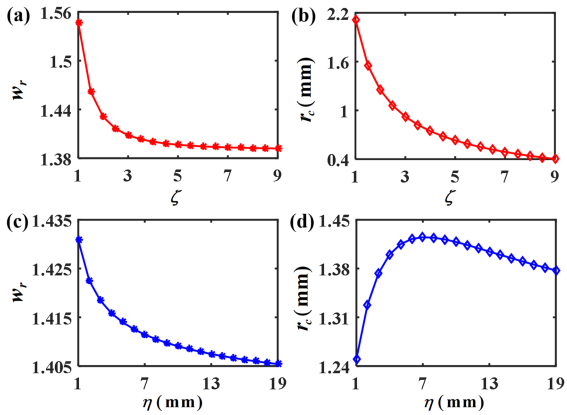


Fig. 4. Influences of anisotropic factor $\zeta$ and inner scale $\eta$ of turbulence on the (a), (c) spreading and (b), (d) wander of asymmetric Bessel-Gaussian beam.

The variations of beam spreading and wander with the anisotropic factor $\zeta$ and inner scale $\eta$ of turbulence eddies are given in Fig. 4. Different from the isotropic case corresponding to $\zeta = 1$, the anisotropic turbulence eddies with $\zeta > 1$ work as focusing lenses to beam propagation [29]. A larger $\zeta$ means stronger anisotropy and higher curvature of these equivalent lenses. With the increment of $\zeta$, the focusing effect makes asymmetric Bessel-Gaussian beam less deviated from the propagation direction. Thus $w_r$ and $r_c$ become smaller especially compared with the isotropic case. In terms of the effects of $\eta$, $w_r$ varies with $\eta$ monotonously while $r_c$ has a maximum. When $\eta$ increases, the turbulence eddies in the inertial range reduce and turbulence perturbation on beam propagation weakens. So $w_r$ and $r_c$ are relatively small in turbulence with large $\eta$. Contrary to the negative effects of turbulence, the aperture smoothing effect

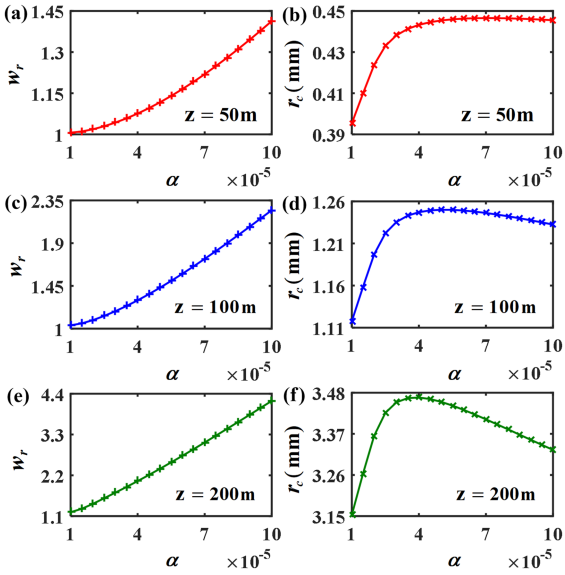


Fig. 5. Influences of beam scale factor $\alpha$ and propagation distance $z$ on the (a), (c), (e) spreading and (b), (d), (f) wander of asymmetric Bessel-Gaussian beam.

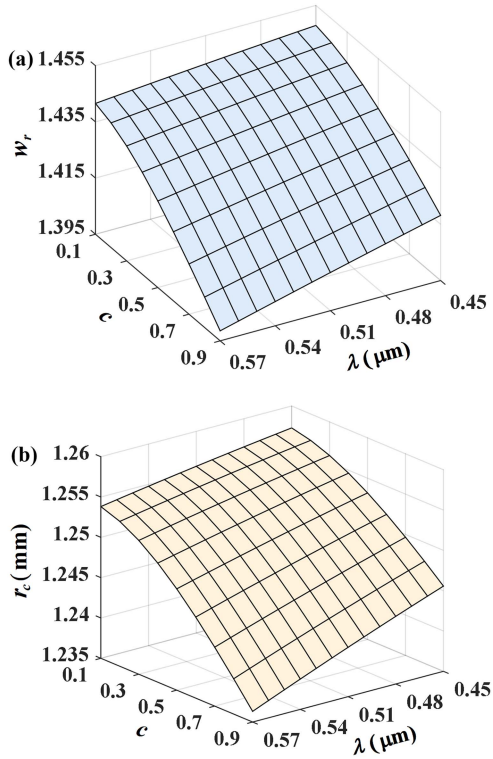


Fig. 6. Influences of wavelength λ and asymmetry factor $c$ on the (a) spreading and (b) wander of asymmetric Bessel-Gaussian beam.

brought by large beam width can mitigate beam wander at the receiver [30]. Since the turbulence perturbation and beam width are both larger when $\eta$ reduces, $r_c$ decreases if the spreading of beam width makes the aperture smoothing effect more dominant than turbulence effect.

Aiming at the impacts of beam parameters, the spreading factor $w_r$ and center displacement $r_c$ of asymmetric Bessel-Gaussian beam under different beam scale factors $\alpha$ are shown in Fig. 5. As for an arbitrary $\alpha$, both $w_r$ and $r_c$ increase with the propagation distance $z$. The increments are significant due to the accumulative effects of beam diffraction and oceanic turbulence. According to the results shown in Fig. 1, the beam with larger $\alpha$ has smaller initial width at the source plane. The smaller transmitted beam has stronger diffraction during propagation. So beam spreading enhances correspondingly and $w_r$ increases with $\alpha$. On the other hand, the beam width at the receiver is determined by the initial width at the transmitter and spreading factor together. The initial width is larger at a smaller $\alpha$ while the spreading factor is larger at a larger $\alpha$. So the received beam width may have a minimum when $\alpha$ is moderate. Since the aperture smoothing effect of wide beam can mitigate the turbulence induced beam wander, $r_c$ shows a trend of rise-fall when $\alpha$ increases.

Fig. 6 gives the spreading and wander of asymmetric Bessel-Gaussian beam under different wavelengths λ and asymmetry factors $c$. Considering the absorption of seawater on beam intensity, blue and green lasers are generally used for underwater propagation due to the lower absorption loss [26]. In the wavelength region of blue and green lasers, longer wavelength corresponds to smaller spreading factor $w_r$ and center displacement $r_c$. This can be attributed to the larger initial width and spatial coherence radius brought by longer wavelength. The beam with larger spatial coherence radius has better immunity to turbulence perturbation.

As a feature parameter of asymmetric Bessel-Gaussian beam, $c$ affects $w_r$ and $r_c$. In the condition of $c/k\alpha < w_0$, the intensity peak of asymmetric Bessel-Gaussian beam deviates more from optical axis with the increment of $c$ [15]. Since beam width is related to intensity distribution, the beam with larger $c$ has larger initial width and then smaller diffraction broadening. Besides, the enhancement of asymmetry brings nonuniform intensity distribution. Most of intensity focuses on a relatively small region and thus suffers less turbulence perturbation. So $w_r$ decreases with the increment of $c$. In spite of the smaller spreading for beam with larger $c$, the beam width at the receiver is still larger due to the larger initial width. The wander of wider beam is weaker, so $r_c$ becomes smaller when $c$ increases. Apart from the reduction of spreading and wander in oceanic turbulence, the increment of $c$ also makes the transverse beam field diverse compared with the circular symmetric field. These advantages make asymmetric Bessel-Gaussian beam potential for different underwater applications where better directionality is needed.

Fig. 7 gives the variations of spreading factor $w_r$ and center displacement $r_c$ with beam order $m$ and the waist radius $w_0$ of Gaussian envelope. According to Fig. 1, the beam width at the source plane increases with $m$. When $w_0$ increases, the initial width of asymmetric Bessel-Gaussian beam also increases. Since the diffraction effect can be weakened by enlarging the transmitted beam width, beam spreading is mitigated effectively with the increment of $m$ and $w_0$ to reduce $w_r$. As for beam wander, $r_c$ monotonously decreases when $m$ and $w_0$ increase. The results are related to the beam width at the receiver. Although the beam with larger $m$ or $w_0$ has smaller spreading, its

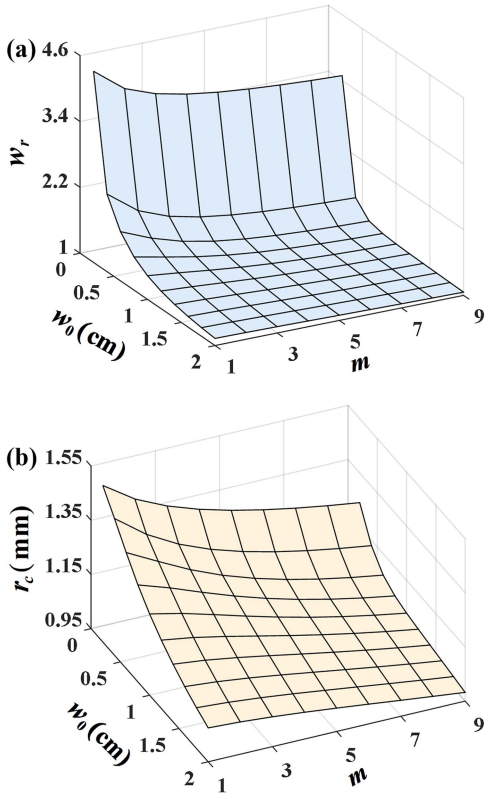


Fig. 7. Influences of beam order $m$ and Gaussian waist radius $w_0$ on the (a) spreading and (b) wander of asymmetric Bessel-Gaussian beam.

larger initial width dominates and results in the larger received width. Due to the smoothing effect of wide beam to turbulence perturbation, beam wander is mitigated. So the selection of a high-order wide beam is helpful to control the spreading and has better directionality for asymmetric Bessel-Gaussian beam.

According to the numerical results, the spreading and wander of asymmetric Bessel-Gaussian beam can be mitigated by ways of beam optimization. The transmission of beam in deeper water with smaller temperature dissipation also suffers less turbulence perturbation. The better directionality helps beam receiving in underwater communications between two submarines or from submarine to surface ship. Besides, the asymmetric vortex beams are also potential for other applications such as turbulence probing and remote sensing [31], [32].

## V. Conclusion

Aiming at the propagation of asymmetric Bessel-Gaussian beam in anisotropic oceanic turbulence, a theoretical model is constructed to investigate beam spreading and wander. By use of cross-spectral density and Wigner distribution function, the long-term beam width is derived to obtain the spreading factor and center displacement. Numerical simulations reveal that the beam suffers less spreading and wander in oceanic turbulence with higher anisotropy, smaller temperature dissipation rate, larger inner scale and kinetic energy dissipation rate. The salinity fluctuation is more negative than temperature fluctuation. From the view of beam optimization, the asymmetric Bessel-Gaussian beam with larger Gaussian waist, smaller beam scale factor, longer wavelength and higher vortex order has less spreading and wander. Improving beam asymmetry is helpful to make the field distribution diverse and directivity better. The results provide references for the investigations of asymmetric vortex beams in turbulent media.

## Appendix

To obtain the analytical expression of $w_l$ in (22), (9) is rewritten as

$$W_{\theta\theta'}(\boldsymbol{r_s}, \boldsymbol{r_d}, z) = \frac{w_0^2}{8\pi} \int_{-\infty}^{\infty} \int_{-\infty}^{\infty} Q_{\theta\theta'}(\boldsymbol{r_d}, \boldsymbol{\kappa_d}, z) \exp(-i\, \boldsymbol{r_s} \cdot \boldsymbol{\kappa_d})\, d^2\, \boldsymbol{\kappa_d}, \tag{A1}$$

$$\begin{aligned} Q_{\theta\theta'}(\boldsymbol{r_d}, \boldsymbol{\kappa_d}, z) &= \exp\left[\frac{i}{2}\, \boldsymbol{k}_+ \cdot \boldsymbol{r_d} + \left(\frac{iz}{2k}\, \boldsymbol{k}_+ - \frac{z\, \boldsymbol{r_d}}{k\, w_0^2} - \frac{w_0^2}{4}\, \boldsymbol{k}_-\right) \cdot \boldsymbol{\kappa_d} \right. \\ &\quad - \left(\frac{w_0^2}{8} + \frac{z^2}{2\, k^2\, w_0^2}\right) \boldsymbol{\kappa_d^2} - \frac{w_0^2}{8}\, \boldsymbol{k}_-^2 - \frac{1}{2}\frac{\boldsymbol{r_d^2}}{w_0^2} \\ &\quad \left. + \psi\left(\boldsymbol{r_d}, \boldsymbol{r_d} + \frac{z}{k}\, \boldsymbol{\kappa_d}, z\right)\right]. \end{aligned} \tag{A2}$$

By substituting (A1) into (17) and using the integral formula given in (20), we can get

$$\begin{aligned} H_{00} &= \frac{1}{2}\pi\, w_0^2\, Q_{\theta\theta'}(0, 0, z) \\ H_{20} + H_{02} &= -\frac{1}{2}\pi\, w_0^2 \\ &\quad \times \left[\left.\frac{\partial^2\, Q_{\theta\theta'}(0, \boldsymbol{\kappa_d}, z)}{\partial\, \boldsymbol{\kappa_{dx}^2}}\right|_{\boldsymbol{\kappa_d}=0} \right. \\ &\quad \left. + \left.\frac{\partial^2\, Q_{\theta\theta'}(0, \boldsymbol{\kappa_d}, z)}{\partial\, \boldsymbol{\kappa_{dy}^2}}\right|_{\boldsymbol{\kappa_d}=0}\right]. \end{aligned} \tag{A3}$$

Conducting the differential operations in (A3) based on the expressions given in (A2) and (11), the result of (21) is obtained.

Then substituting (21) into (18) and conducting the integral operations by use of the following formulae [20]:

$$\begin{aligned} &\int_0^{2\pi} \exp\left[in\theta + \tau\cos(\theta - \varphi)\right] d\theta = 2\pi I_n(\tau) \exp(in\varphi) \\ &\int_0^{2\pi} \exp(in\theta)\mathrm{d}\theta = 2\pi\delta(n)[n \in N], \end{aligned} \tag{A4}$$

the result is written as

$$\begin{aligned} S_{00} &= \tfrac{1}{2}\pi\, w_0^2 \exp\left(-\tfrac{w_0^2}{4}\, \alpha^2\, k^2\right) \sum_{p=0}^{\infty} \tfrac{|c|^{2p}}{p!^2}\, I_{m+p}\left(\tfrac{\alpha^2\, k^2\, w_0^2}{4}\right) \\ S_{20} + S_{02} &= \left[\tfrac{w_0^2}{2} - \tfrac{w_0^4}{8}\, \alpha^2\, k^2 + \left(\tfrac{\alpha^2}{2} + \tfrac{2}{k^2\, w_0^2} + \tfrac{4}{k^2\, \rho_c^2}\right) z^2\right] \\ &\quad \times S_{00} + \tfrac{1}{2}\pi\, w_0^2 \left(\tfrac{\alpha^2\, z^2}{4} + \tfrac{\alpha^2\, k^2\, w_0^4}{16}\right) \exp\left(-\tfrac{w_0^2}{4}\, \alpha^2\, k^2\right) \\ &\quad \times \sum_{p=0}^{\infty} \tfrac{|c|^{2p}}{p!^2} \left[I_{m+p+1}\left(\tfrac{\alpha^2\, k^2\, w_0^2}{4}\right) + I_{m+p-1}\left(\tfrac{\alpha^2\, k^2\, w_0^2}{4}\right)\right]. \end{aligned} \tag{A5}$$

After substituting (A5) into (19), the expression of $w_l$ is simplified as the form in (22).

To calculate the integration in (25), we extend (25) with the expression given by (13) as

$$\begin{aligned} R(\sigma) = {} & 0.388 \times 10^{-8} \chi_T \varepsilon^{-1/3} \zeta^{-2} \varpi^{-2} \\ & \times \int_0^{\infty} \kappa_\zeta^{-2/3} d\,\kappa_\zeta \left[ \varpi^2 \exp\left(-\,U_1\,\kappa_\zeta^{4/3}\right.\right. \\ & \left. - V_1\,\kappa_\zeta^2\right) - 2\varpi \exp\left(-\,U_2\,\kappa_\zeta^{4/3} - V_2\,\kappa_\zeta^2\right) \\ & \left. + \exp\left(-\,U_3\,\kappa_\zeta^{4/3} - V_3\,\kappa_\zeta^2\right)\right] \\ & + 0.912 \times 10^{-8} \chi_T \varepsilon^{-1/3} \zeta^{-2} \eta^{2/3} \varpi^{-2} \\ & \int_0^{\infty} d\,\kappa_\zeta \left[ \varpi^2 \exp\left(-\,U_1\,\kappa_\zeta^{4/3}\right.\right. \\ & \left. - V_1\,\kappa_\zeta^2\right) - 2\varpi \exp\left(-\,U_2\,\kappa_\zeta^{4/3} - V_2\,\kappa_\zeta^2\right) \\ & \left. + \exp\left(-\,U_3\,\kappa_\zeta^{4/3} - V_3\,\kappa_\zeta^2\right)\right], \end{aligned} \tag{A6}$$

where the terms $U_i$ and $V_i (i = 1, 2, 3)$ are written as (28). The integral results can be obtained with the help of the following formulae [33], [34]:

$$\begin{aligned} & \int_0^{\infty} \kappa^{2n-8/3} \exp\left(-\,U\kappa^{4/3} - V\kappa^2\right) d\kappa = \tfrac{1}{4} V^{-1/2-n} \\ & \times \left[ 2V^{4/3} \Gamma\left(n - \tfrac{5}{6}\right) {}_2F_2\left(\tfrac{n}{2} - \tfrac{5}{12}, \tfrac{n}{2} + \tfrac{1}{12}; \tfrac{1}{3}, \tfrac{2}{3}; -\tfrac{4U^3}{27V^2}\right)\right. \\ & -2UV^{2/3} \Gamma\left(n - \tfrac{1}{6}\right) {}_2F_2\left(\tfrac{n}{2} - \tfrac{1}{12}, \tfrac{n}{2} + \tfrac{5}{12}; \tfrac{2}{3}, \tfrac{4}{3}; -\tfrac{4U^3}{27V^2}\right), \\ & \left. +U^2 \Gamma\left(n + \tfrac{1}{2}\right) {}_2F_2\left(\tfrac{n}{2} + \tfrac{1}{4}, \tfrac{n}{2} + \tfrac{3}{4}; \tfrac{4}{3}, \tfrac{5}{3}; -\tfrac{4U^3}{27V^2}\right)\right] \end{aligned} \tag{A7}$$

$$\begin{aligned} & \int_0^{\infty} \kappa^{2n-2} \exp\left(-\,U\kappa^{4/3} - V\kappa^2\right) d\kappa = \tfrac{1}{4} V^{-5/6-n} \\ & \times \left[ 2V^{4/3} \Gamma\left(n - \tfrac{1}{2}\right) {}_2F_2\left(\tfrac{n}{2} - \tfrac{1}{4}, \tfrac{n}{2} + \tfrac{1}{4}; \tfrac{1}{3}, \tfrac{2}{3}; -\tfrac{4U^3}{27V^2}\right)\right. \\ & -2UV^{2/3} \Gamma\left(n + \tfrac{1}{6}\right) {}_2F_2\left(\tfrac{n}{2} + \tfrac{1}{12}, \tfrac{n}{2} + \tfrac{7}{12}; \tfrac{2}{3}, \tfrac{4}{3}; -\tfrac{4U^3}{27V^2}\right), \\ & \left. +U^2 \Gamma\left(n + \tfrac{5}{6}\right) {}_2F_2\left(\tfrac{n}{2} + \tfrac{5}{12}, \tfrac{n}{2} + \tfrac{11}{12}; \tfrac{4}{3}, \tfrac{5}{3}; -\tfrac{4U^3}{27V^2}\right)\right] \end{aligned} \tag{A8}$$

where $\Gamma(\cdot)$ is the Gamma function, ${}_2F_2(\cdot)$ is the generalized hypergeometric function. According to the asymptotic relation ${}_2F_2(a, b; f, g; -x) \approx 1 - abx/fg, |x| \ll 1$, the simplified expression of (A6) is written as

$$\begin{aligned} R(\sigma) = {} & 0.194 \times 10^{-8} \chi_T \varepsilon^{-1/3} \zeta^{-2} \\ & \times \left(A'_1 - 2A'_2 \varpi^{-1} + A'_3 \varpi^{-2}\right) \\ & + 0.456 \times 10^{-8} \chi_T \varepsilon^{-1/3} \zeta^{-2} \eta^{2/3} \\ & \times \left(A''_1 - 2A''_2 \varpi^{-1} + A''_3 \varpi^{-2}\right) \\ A'_i = {} & \Gamma(1/6)\, V_i^{-1/6} - \Gamma(5/6)\, U_i\, V_i^{-5/6} \\ & + 0.5\Gamma(3/2)\, U_i^2\, V_i^{-3/2} \\ A''_i = {} & \Gamma(1/2)\, V_i^{-1/2} - \Gamma(7/6)\, U_i\, V_i^{-7/6} \\ & + 0.5\Gamma(11/6)\, U_i^2\, V_i^{-11/6}, \end{aligned} \tag{A9}$$

where $i = 1, 2, 3$, the values of function terms ${}_2F_2(\cdot)$ related to $U_i$ and $V_i$ are approximated as the constant 1 with errors negligible. Then calculating the values of function terms $\Gamma(\cdot)$ in (A9), the final result of $R(\sigma)$ given by (26) and (27) is obtained.

## REFERENCES


[1] P. Ju et al., "Atmospheric turbulence effects on the performance of orbital angular momentum multiplexed free-space optical links using coherent beam combining," *Photonics*, vol. 10, no. 6, Jun. 2023, Art. no. 634.

[2] L. Andrews and R. Philips, *Laser Beam Propagation Through Random Media*. Bellingham, WA, USA: SPIE Press, 2005.

[3] V. Lukin, P. Konyaev, and V. Sennikov, "Beam spreading of vortex beams propagating in turbulent atmosphere," *Appl. Opt.*, vol. 51, no. 10, pp. C84–C87, Apr. 2012.

[4] Y. Wu, Y. Zhang, Y. Li, and Z. Hu, "Beam wander of Gaussian-Schell model beams propagating through oceanic turbulence," *Opt. Commun.*, vol. 371, pp. 59–66, Jul. 2016.

[5] L. Cui and L. Cao, "Theoretical expressions of long term beam spread and beam wander for Gaussian wave propagating through generalized atmospheric turbulence," *Optik*, vol. 126, no. 23, pp. 4704–4707, Dec. 2015.

[6] B. Zhang, Y. Xu, X. Wang, and Y. Dan, "Propagation factor and beam wander of electromagnetic Gaussian Schell-model array beams in non-Kolmogorov turbulence," *OSA Continuum*, vol. 2, no. 1, pp. 162–174, Jan. 2019.

[7] Y. Jin et al., "Beam wander of a partially coherent Airy beam in oceanic turbulence," *J. Opt. Soc. Amer. A*, vol. 35, no. 8, pp. 1457–1464, Aug. 2018.

[8] Y. Ata, Y. Baykal, and M. Gökçe, "Analysis of wander and spreading of an optical beam by using the oceanic turbulence optical power spectrum," *J. Opt. Soc. Amer. B*, vol. 39, no. 8, pp. 2129–2137, Aug. 2022.

[9] Y. Bai, H. Lv, X. Fu, and Y. Yang, "Vortex beam: Generation and detection of orbital angular momentum," *Chin. Opt. Lett.*, vol. 20, no. 1, Jan. 2022, Art. no. 012601.

[10] K. Zhu, S. Li, Y. Tang, Y. Yu, and H. Tang, "Study on the propagation parameters of Bessel–Gaussian beams carrying optical vortices through atmospheric turbulence," *J. Opt. Soc. Amer. A*, vol. 29, no. 3, pp. 251–257, Mar. 2012.

[11] C. Luo and X. Han, "Evolution and beam spreading of arbitrary order vortex beam propagating in atmospheric turbulence," *Opt. Commun.*, vol. 460, Apr. 2020, Art. no. 124888.

[12] S. Singh, S. Mishra, and A. Mishra, "Ring Pearcey vortex beam dynamics through atmospheric turbulence," *J. Opt. Soc. Amer. B*, vol. 40, no. 9, pp. 2287–2295, Sep. 2023.

[13] A. Falits, V. Kuskov, and V. Banakh, "Propagation of vortex optical beams through artificial convective turbulence," *J. Quantitative Spectrosc. Radiative Transfer*, vol. 302, Jul. 2023, Art. no. 108568.

[14] H. Yang, Y. Zhang, G. Zhao, L. Yu, and L. Hu, "Wander and spread of a perfect Laguerre–Gauss beam under turbulent absorbent seawater," *Appl. Opt.*, vol. 61, no. 15, pp. 4549–4557, May 2022.

[15] V. Kotlyar, A. Kovalev, R. Skidanov, and V. Soifer, "Asymmetric Bessel-Gauss beams," *J. Opt. Soc. Amer. A*, vol. 31, no. 9, pp. 1977–1983, Sep. 2014.

[16] V. Kotlyar, A. Kovalev, and A. Porfirev, "Asymmetric Gaussian optical vortex," *Opt. Lett.*, vol. 42, no. 1, pp. 139–142, Jan. 2017.

[17] K. Dai et al., "Second-harmonic generation of asymmetric Bessel-Gaussian beams carrying orbital angular momentum," *Opt. Exp.*, vol. 28, no. 2, pp. 2536–2546, Jan. 2020.

[18] Q. Wu and Z. Ren, "Study of the nonparaxial propagation of asymmetric Bessel–Gauss beams by using virtual source method," *Opt. Commun.*, vol. 432, pp. 8–12, Feb. 2019.

[19] L. Yu, Y. Zhang, and J. Wang, "Propagation of asymmetric Bessel mode in turbulent atmosphere," *IEEE Photon. J.*, vol. 14, no. 5, Oct. 2022, Art. no. 7354106.

[20] I. Gradshteyn and I. Ryzhik, *Table of Integrals, Series, and Products*. Burlington, VT, USA: Academic Press, 2007.

[21] Y. Dan and B. Zhang, "Beam propagation factor of partially coherent flat-topped beams in a turbulent atmosphere," *Opt. Exp.*, vol. 16, no. 20, pp. 15563–15575, Sep. 2008.

[22] V. V. Nikishov and V. I. Nikishov, "Spectrum of turbulence fluctuations of the sea-water refraction index," *Int. J. Fluid Mechanics Res.*, vol. 27, no. 1, pp. 82–98, Jan. 2000.

[23] X. Huang, Z. Deng, X. Shi, Y. Bai, and X. Fu, "Average intensity and beam quality of optical coherence lattices in oceanic turbulence with anisotropy," *Opt. Exp.*, vol. 26, no. 4, pp. 4786–4797, Feb. 2018.

[24] R. Castañeda, "On the relationship between the cross-spectral density and the Wigner distribution function," *J. Modern Opt.*, vol. 45, no. 3, pp. 587–593, Mar. 1998.

[25] Y. Baykal, Y. Ata, and M. Gökçe, "Underwater turbulence, its effects on optical wireless communication and imaging: A review," *Opt. Laser Technol.*, vol. 156, Dec. 2022, Art. no. 108624.

[26] Z. Vali, A. Gholami, Z. Ghassemlooy, M. Omoomi, and D. Michelson, "Experimental study of the turbulence effect on underwater optical wireless communications," *Appl. Opt.*, vol. 57, no. 28, pp. 8314–8319, Oct. 2018.

[27] Z. Wang, L. Lu, P. Zhang, C. Fan, and X. Ji, "Broadening of ultrashort pulses propagating through weak-to-strong oceanic turbulence," *Opt. Commun.*, vol. 367, pp. 95–101, May 2016.

[28] S. Thorpe, *The Turbulent Ocean*. Cambridge, MA, USA: Cambridge Univ. Press, 2005.

[29] I. Toselli, B. Agrawal, and S. Restaino, "Light propagation through anisotropic turbulence," *J. Opt. Soc. Amer. A*, vol. 28, no. 3, pp. 483–488, Mar. 2011.

[30] Y. Fu, Q. Duan, C. Huang, Y. Du, and L. Zhou, "Average BER performance of rectangular QAM-UWOC over strong oceanic turbulence channels with pointing error," *Opt. Commun.*, vol. 476, Dec. 2020, Art. no. 126362.

[31] R. Watkins et al., "Experimental probing of turbulence using a continuous spectrum of asymmetric OAM beams," *Opt. Exp.*, vol. 28, no. 2, pp. 924–935, Jan. 2020.

[32] K. Dai, J. Miller, J. Free, M. Lemon, F. Dalgleish, and E. Johnson, "Remote sensing using a spatially and temporally controlled asymmetric perfect vortex basis generated with a 2D HOBBIT," *Opt. Exp.*, vol. 30, no. 19, pp. 34765–34775, Sep. 2022.

[33] L. Lu, X. Ji, and Y. Baykal, "Wave structure function and spatial coherence radius of plane and spherical waves propagating through oceanic turbulence," *Opt. Exp.*, vol. 22, no. 22, pp. 27112–27122, Nov. 2014.

[34] Y. Pan et al., "Propagation properties of rotationally-symmetric power-exponent-phase vortex beam through oceanic turbulence," *Opt. Laser Technol.*, vol. 159, Apr. 2023, Art. no. 109024.